RESEARCH ARTICLE

Remote Estimation of the Chlorophyll-a Concentration in Lake Dianshan, China Using High-Spatial-Resolution Satellite Imagery

Xiaoman Lu[1,2] · Chunyan Situ[1] · Jiajia Wang[1] · Liguo Zhou[1,2,3] · Weichun Ma[1] · Linna Li[4]

Abstract

The high spatial resolution of satellite data and the capability of physics-based approaches are considered highly suitable for testing the integration of remote sensing technologies into the water quality monitoring of small and medium-sized inland lakes. This research thus aimed to investigate an operational algorithm for chlorophyll-a (Chla) estimation based on China's recently launched high-spatial-resolution GF-1 satellite data for Lake Dianshan, a eutrophic lake in Shanghai city, eastern China. For the calibration of the empirical model, an enhanced three-band model and an improved four-band model (IFB) developed by model derivation and statistical analysis based on in situ water sampling and satellite reflectance data were proposed. The IFB model could account for more than 90% of the Chla variation in the GF-1 satellite data. For the calibration of the semi-empirical model, the performance of $\Delta\Phi$ and an improved NCI model (NCI') were analyzed and validated with field spectral measurements and GF-1 satellite data. The corresponding GF-1 satellite $\Delta\Phi$ model and NCI' model reached high estimation accuracies of $R^2 = 0.80$ and 0.76, respectively. The good estimated results indicate that the established GF-1 satellite models are promising and applicable to estimating Chla in small and medium-sized eutrophic inland lakes.

Keywords GF-1 satellite · High spatial resolution · Chlorophyll-a · Semi-empirical model

Introduction

The eutrophication of inland lake water has become a significant environmental problem, which leads to many restrictions on water resource utilization (Zhou et al., 2014). The chlorophyll-a (Chla) concentration is one of the most important water quality parameters (WQPs) for measuring the trophic state of lake water (Arabi et al., 2016; Schalles, 1998). For the remote estimation of Chla in small and medium-sized inland lakes, the spatial resolution of satellite data should be the first factor to be considered because of the limited lake area and the variation in WQPs (Fichot et al., 2016; González Vilas et al., 2011; Kloiber et al., 2002).

At present, high-spatial-resolution satellite imagery has been widely used in many study areas, such as land use classification, atmospheric pollution monitoring, and archaeological investigations (Lin et al., 2015; Myint et al., 2011; Sarris et al., 2013). However, there is a lack of relevant studies on high-spatial-resolution satellite data, such as those from RapidEye, Ikonos, and QuickBird, applied to water quality monitoring of small to medium-sized inland lakes (Choe et al., 2015; Ekercin, 2007; Wu & Cheng, 2010).

GaoFen-1 (GF-1), the first Chinese high-spatial-resolution satellite system, was launched on April 26, 2013, and March 31, 2018; it consists of four satellites, which are equipped with two 2 m panchromatic/8 m multispectral cameras and four 16 m-wide field-of-view imagers (WFV). The swath width of the 16 m WFV reaches to 800 km, which makes this sensor a good choice for water quality monitoring of small and medium-sized inland lakes, and enables it to monitor several water bodies at the same time

✉ Liguo Zhou
Lgzhou@fudan.edu.cn

[1] Department of Environmental Science and Engineering, Fudan University, Shanghai 200433, China

[2] Key Laboratory of Spatial-Temporal Big Data Analysis and Application of Natural Resources in Megacities, MNR, Shanghai 200063, China

[3] Institute of Eco-Chongming (IEC), No. 3663 Northern Zhongshan Road, Shanghai 200062, China

[4] Department of Geography, California State University, Long Beach, CA 90840, USA

(Yang et al., 2015). Additionally, the revisit time is only four days, and the GF-1 satellite data are available free of charge and can thus meet the requirements of routine water quality monitoring for similar studies. Until now, researchers have tried to build several kinds of models for estimating Chla, TSS, transparency, and eutrophication indexes with GF-1 satellite data (Li et al., 2015; Tian et al., 2016; Wu et al., 2015). However, the model accuracy still needs improvement to enable the use of such multiband high-spatial-resolution satellite data, and powerful and sufficiently accurate algorithms that can explore the great potential of GF-1 satellite data for water quality monitoring should be investigated.

In general, the algorithms used for Chla estimation in water bodies with remote sensing technology can be divided into three classes: (1) The empirical approach is based on the development of bivariate or multivariate regressions between Chla concentrations measured in situ and remote sensing data (i.e., satellite band reflectance, band ratio or other band combinations) (Allan et al., 2015). (2) The bio-optical algorithm, with the principle of retrieving the Chla concentration based on the inherent optical properties of water, claims to be more universal for water quality monitoring; however, it requires more situ physical parameters which are difficult to obtain for researchers (Dall'Olmo and Gitelson 2005; Giardino et al., 2014; Zhou et al., 2015). (3) The semi-empirical algorithm is essentially a simplified bio-optical model in which the spectral characteristics of the WQPs of interest are known. Statistical analysis is included to determine the appropriate wavelengths within a well-chosen spectral range (Feng et al., 2015; Watanabe et al., 2016; Zhou et al., 2014). The superiority of the semi-empirical model is expressed in its satisfactory accuracy and easily obtained parameters, which is suitable for GF-1 satellite data.

The objective of this study was to investigate an operational model for estimating the concentration of Chla in small and medium-sized lakes based on GF-1 satellite imagery. The specific aims were to build satellite estimation models through formula derivation and statistical analysis and compare the accuracy and sensitivity of the established models that attained satisfactory model accuracy. In addition, spatial analysis of the Chla concentrations was conducted based on the satellite-derived estimation in Lake Dianshan, China.

## Study Area and Data Processing

Study Area

Lake Dianshan (30° 12′–31° 04′ N and 120° 54′–121° 01′ E) was selected as the case study area. It is located in the upper catchment of the Huangpu River, Shanghai, an international metropolis of China (Fig. 1). It is a eutrophic and shallow freshwater lake, the average depth is 2.11 m, and the surface area covers approximately 62 km^2 (Zhou et al., 2013). As the most important water source of the Huangpu River, Lake Dianshan supplies more than 60% of the domestic water and industrial water for Shanghai city. Additionally, Lake Dianshan plays an important role in climate regulation, farmland irrigation, and water transportation (Zou et al., 2013). Since the end of the last century, the concentrations of nitrogen and phosphorus in the lake have continuously increased (Xiong et al., 2017). In the summer of 2007, an algal bloom extended to more than 80% of the lake area. In recent years, the eutrophic conditions in Lake Dianshan also pose a large risk to human health and the safety of the residents of Shanghai city (Liu et al., 2014).

Field Data and Laboratory Analysis

Based on the direction of water flow and the need for a uniform distribution of sampling points, 13 routine sampling sites were set up in the lake. The spatial distribution of the sampling points is shown in Fig. 1; site 9 and site 1 were the main inlet and outlet of the lake water, respectively. Thirty-nine samples were collected on December 4rd, 2013; May 8th, 2014; and January 9th, 2015 (13 samples per day) when the GF-1 satellite passed over at 10:30 A.M. in sun synchronous orbit. To synchronize the data measured in situ with the satellite data, the water samples and field spectral measurements were collected from 10:00 to 12:00 A.M. local time. The latitude and longitude of each sample site were determined by handheld high-precision GPS.

Field spectral reflectance was measured with an ASD FieldSpec Spectroradiometer. This instrument has a sensitivity range from 350 to 1075 nm and a spectral resolution of 1.5 nm. During the field measurements, the instrument was held with a field view of 25°, approximately 1 m above the water surface (Zhou et al., 2015). The angle between the instrument observation and the plane of the incident radiation from the sun was maintained at 90°–135°, so that most of the direct sunlight was eliminated and the impact of the ship's shadow was minimized. The spectra in each sampling station were measured at least ten times, and a mean value was taken as the result. In this study, 30 field spectral measurements were obtained in Lake Dianshan on Sept. 7th–8th, 2010. The lake is a typical case-2 water body, and it showed a low water transparency (average < 0.5 m) in the field measurement. Thus, spectral measurements are unlikely to be influenced by the reflectance from the lake bottom (Zhou et al., 2014).
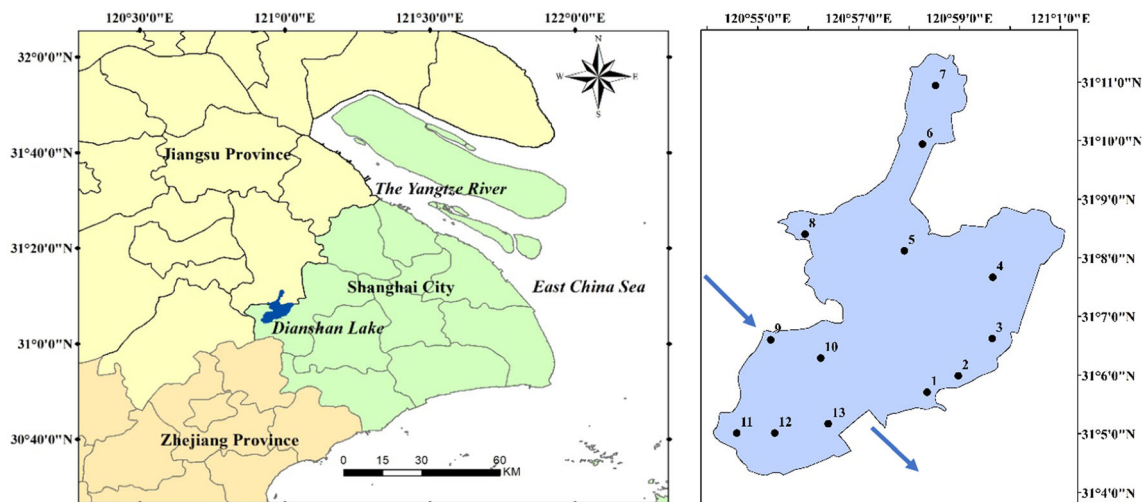
Fig. 1 **a** Geographical location of the study area (The vector map is downloaded from the website of National Geomatics Center of China: https://www.webmap.cn/). **b** Spatial locations of the sampling sites in Lake Dianshan (The arrow represents the direction of water flow in the lake)

The water samples were collected from a depth of 50 cm to the water surface, and the water sample collection and storage were in full accordance with the standards (HJ493-2009) issued by the Chinese Environmental Protection Administration (http://www.mee.gov.cn/). The concentration of Chla was measured in the laboratory using the spectrophotometric method. First, the 1 L water samples were filtered through 0.45 μm GF/C filters, left at 4 °C for 24 h in the dark, and then extracted by 95% acetone. After centrifugation, a UV-2501 spectrophotometer was used to measure the extinction values at 630 nm, 645 nm, 663 nm, and 750 nm. Finally, the concentration of Chla was calculated using equations from the Scientific Committee on Oceanic Research-United Nations Educational, Scientific and Cultural Organization (Gons, 2005). The Chla concentrations of the 30 samples used to calibrate the field spectral semi-analytical model ranged from 5.53 to 100.3 μg/L, with an average of 27.74 μg/L. Moreover, the Chla concentrations of the 39 water samples used for the satellite modeling ranged from 1.51 to 39.80 μg/L, with an average of 17.34 μg/L, as shown in Table 1.

GF-1 Satellite Data and Image Preprocessing

GF-1 Satellite Data

GF-1 satellite images were acquired from the website of the China Centre for Resources Satellite Data and Application (http://www.cresda.com/CN/). In our study, three temporal GF-1 WFV2 satellite images for satellite modeling were obtained on December 4th, 2013; May 8th, 2014; and January 9th, 2015. The spectral range of the GF-1 WFV2 sensor covers from 450 to 890 nm (Table S1), including four broadband channels: 450–520 nm (B_1),

520–590 nm (B_2), 630–690 nm (B_3), and 770–890 nm (B_4).

Image Preprocessing

(1)   Geometric correction

A preliminary geometric correction based on the provided rational polynomial coefficients (RPC) was carried out for the GF-1 satellite images. Then, the satellite images were further geometrically rectified with a topographic map (1:50,000) using Exelis Visual Information Solutions (ENVI, version 5.2) software. Nearest-neighbor interpolation was used to avoid disturbance in the original radiometric values. The root mean square error (RMSE) of the satellite images was within 0.5 pixels after the geometric correction processes (Sun et al., 2013).

(2)   Radiometric calibration

The purpose of radiometric calibration is to transform the GF-1 satellite sensor observation values (DN) to the corresponding physical-based radiometric intensity values (Han et al., 2014; Yang et al., 2015). ENVI software 5.1 was used to achieve the by-band calibration based on the absolute calibration coefficients of each band. The equation used is shown in Eq. (1).

$$Lr = Gain * DN + Bias \qquad (1)$$

In this equation, Lr is the radiometric value, Gain and Bias represent the gain coefficient and bias value of each band, respectively, and the unit of Lr is $W \cdot m^{-2} \cdot sr^{-1} \cdot \mu m^{-1}$. All gain coefficients and bias coefficients can be found on the China Centre for Resources Satellite Data and Application website (http://www.cresda.com/CN/Downloads/dbcs/ index.shtml).

Table 1 GF-1 satellite data and field spectral measurements

Remote sensing data	In situ measurements	Date of GF-1 images	Number	Chla (µg/L)		
				Min	Max	Mean
GF-1 satellite data	20,131,203	20,131,204	13	1.51	10.70	4.53
	20,140,505	20,140,508	13	5.53	32.90	18.36
	20,150,108	20,150,109	13	10.50	39.80	30.19
Field spectral measurements	20,100,908	–	17	10.06	70.53	30.29
	20,100,907	–	13	5.53	100.3	24.41

(3)   Atmospheric correction

The GF-1 satellite images were atmospherically corrected using the MODTRAN-based FLAASH procedure in ENVI 5.1 software to obtain satellite reflectance values (Choe et al., 2015; Wu et al., 2015). The input parameters for the FLAASH module included the information of the GF-1 WFV sensor itself, Greenwich Mean Time of the image acquisition, the average digital elevation of the sensor, visibility, atmospheric model, and aerosol model. In this procedure, the height of the GF-1 sensor was approximately 645 km, and the solar elevation angle and solar azimuth angle were read from the header file of the GF-1 satellite data. Atmospheric visibility data were obtained from the Shanghai Meteorological Bureau. The atmospheric model used was based on the imagery date; for example, the midlatitude summer atmospheric model with an urban aerosol type was used for the image acquired on May 8th, 2014.

Chla Estimation Methods

In this study, empirical and semi-empirical models were investigated to estimate the Chla concentrations in Lake Dianshan based on GF-1 satellite reflectance and field spectral measurements. For the satellite data modeling, the Chla measured in 3 days were sorted, and the 39 samples were divided into two parts: 2/3 of the samples were used for model calibration, and the other 1/3 of the samples were used for model evaluation.

The Enhanced Three-Band (ETB) Model

The typical three-band model has been widely used due to its high model accuracy (Chen et al., 2013; Duan et al., 2010). Because the band setting of the GF-1 WFV2 sensor cannot fully meet the requirements of the three-band model, the three-band model cannot be directly applied. Studies have shown that the third band (459–479 nm) and the fourth band (545–565 nm) of the MODIS satellite

could explain the variance in TSS and CDOM (Hu et al., 2004). To improve the accuracy of the three-band model for GF-1 satellite data, the product of the blue band (450–520 nm) and the green band (520–590 nm) of the GF-1 satellite was selected as a substitute for λ_2 to decrease the influence of TSS and CDOM. Therefore, the ETB model of GF-1 satellite data takes the following form:

$$\text{Chla} \propto \left(R^{-1}(B_3) - R^{-1}(B_1 \times B_2) \right) \cdot R(B_4) \qquad (2)$$

The Improved Four-Band (IFB) Model

The newly developed four-band model makes full use of the information from four different bands and shows good estimation accuracy (Le et al., 2009). However, the wavelength used in the four-band model does not fall within the coverage of the four GF-1 bands. Considering the band setting of GF-1 satellite data, an optimal four-band model (IFB model) was investigated, because the estimations of this model generated the highest correlation with the Chla concentrations measured in situ (Feng et al., 2015; Ma & Dai, 2005).

$$\text{Chla} \propto \left(R^{-1}(B_1) + R^{-1}(B_2) \right) / \left(R^{-1}(B_3) + R^{-1}(B_4) \right)^{0.5}$$
$$(3)$$

$\Delta\Phi$ Model

Hu et al. (2004) proposed a Chla retrieval model based on MODIS satellite data for water quality monitoring in Tampa Bay:

$$\Delta\phi = \frac{[R(\lambda_{555}) - R(\lambda_{859})] / [R(\lambda_{469}) - R(\lambda_{859})]}{[R(\lambda_{555}) - 0.0145] / [R(\lambda_{645}) - 0.008]} \qquad (4)$$

In terms of the band setting of GF-1 satellite sensors, we attempt to apply the $\Delta\Phi$ model for the estimation of Chla in our study area to further explore the applicability and accuracy of this model. Therefore, the specific form of the $\Delta\Phi$ model based on GF-1 satellite data is shown as follows:

$$\Delta\phi = \frac{[R(B_2) - R(B_4)]/[R(B_1) - R(B_4)]}{[R(B_2) - 0.0145]/[R(B_3) - 0.008]} \tag{5}$$

The NCI' Model

For case-2 water bodies, Cheng et al. (2013) developed an NCI model and applied it to estimate Chla in Taihu Lake. The model was formulated as $NCI = [R(\lambda_{690})/R(\lambda_{550}) - R(\lambda_{675})/R(\lambda_{700})]/[R(\lambda_{690})/R(\lambda_{550}) + R(\lambda_{675})/R(\lambda_{700})]$. Moreover, the NCI model has been adapted for satellite retrieval of Chla in optically complex water bodies, and the model has shown high accuracy and stability compared with the typical three-band model or four-band model.

To further improve the applicability of the NCI model for GF-1 satellite data, based on the band reflectance characteristics of the GF-1 satellite sensor, the band difference of $R(B_4) - R(B_1)$ showed a high correlation with the in situ Chla concentrations and was selected to set up the NCI' model. Therefore, the NCI' model that is suitable for GF-1 satellite data can be shown as follows:

$$NCI' = \frac{R(B_3)/R(B_2) - [R(B_4) - R(B_1)]}{R(B_3)/R(B_2) + [R(B_4) - R(B_1)]} \tag{6}$$

Model Accuracy Assessment

Four indexes were used to evaluate model performance: the coefficient of determination (R^2), relative error (RE), mean absolute percentage error ($MAPE$), and $RMSE$ (Chen et al., 2013; Watanabe et al., 2015). The indexes are defined by Eqs. (7–10):
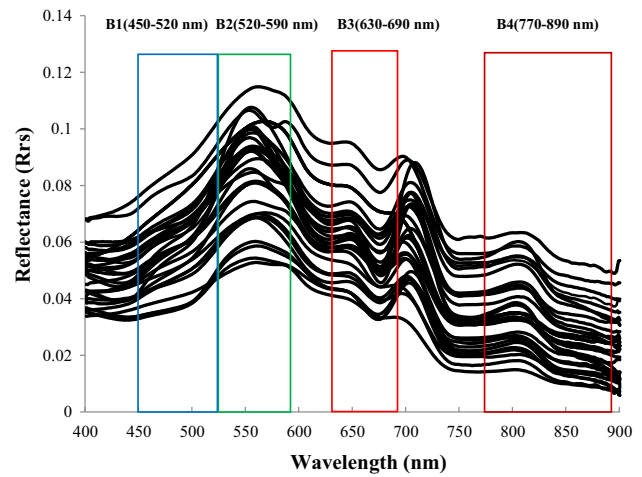

Fig. 2 The field spectra were measured with an ASD FieldSpec Spectroradiometer and the band locations of the GF-1 satellite data

where n is the number of samples, $Chla_{est}$ is the estimated concentration of Chla, and $Chla_{insitu}$ is the Chla concentration measured in situ.

Results and Analysis

Field Spectral Characteristics

Figure 2 shows the field reflectance spectra measured in the Dianshan Lake on Sept. 7th–8th, 2010. According to the band setting of the GF-1 satellite data, the wavelengths that are sensitive to Chla are mainly included by the band locations of the GF-1 satellite data. The low reflectance is between 450 and 520 nm, corresponds to band 1 of

$$R^2 = \frac{\sum_{i=1}^{n}\left(Chl-a_{in\,situ} - \overline{Chl-a_{in\,situ}}\right)^2 - \sum_{i=1}^{n}\left(Chl-a_{in\,situ} - Chl-a_{est}\right)^2}{\sum_{i=1}^{n}\left(Chl-a_{in\,situ} - \overline{Chl-a_{in\,situ}}\right)^2} \tag{7}$$

$$RE = \left|\frac{Chla_{est} - Chla_{in\,situ}}{Chla_{in\,situ}}\right| * 100\% \tag{8}$$

$$MAPE = \frac{\sum_{i=1}^{n}|(Chla_{est} - Chla_{in\,situ})/Chla_{in\,situ}|}{n} * 100\% \tag{9}$$

$$RMSE = \sqrt{\frac{\sum_{i=1}^{n}(Chla_{est} - Chla_{in\,situ})^2}{n}} \tag{10}$$

the GF-1 WFV sensor (Ma & Dai, 2005). The spectra are much higher at approximately 560 nm, which locates at the center of band 2 of GF-1, as a result of minimum absorption by pigments and high backscattering by inorganic suspended matter (Zhou et al., 2014). Moreover, the strong absorption by Chla generates a significant reflectance trough around 675 nm corresponding to band 3 of the GF-1 sensor. In the NIR region of the spectrum located at band 4 of GF-1, reflectance is mostly controlled by the scattering of all particulate matters (Carter & Knapp, 2001; Gitelson et al., 2008).
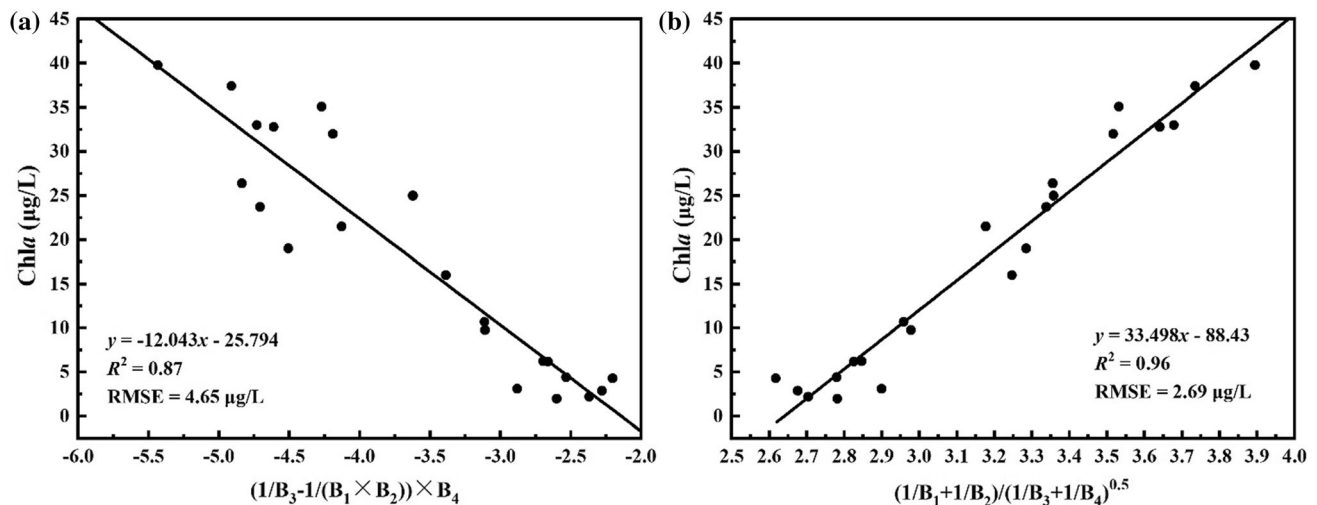
Fig. 3 The calibration of multiband combined model based on GF-1 satellite data: **a** calibration of the ETB model; **b** calibration of the IFB model

Model Calibration

The modeling results of the ETB model based on GF-1 images are shown in Fig. 3a. The coefficient of determination of the ETB model reached 0.87, which is higher than that of the band ratio model ($R^2 = 0.63$). Therefore, the ETB model is acceptable for the quantitative estimation of the Chla concentration. In contrast, the Chla concentrations estimated by the IFB model are shown in Fig. 3b. The coefficient of the IFB model reached 0.96, which indicated significant performance.

Figure 4a shows the modeling result of the linear $\Delta\Phi$ model constructed by using GF-1 satellite data. The satellite $\Delta\Phi$ model had a good fitting degree, and the coefficient of the determination reached 0.80, which indicates a good reflection of the relationship between the satellite reflectance and the concentration of Chla. Figure 4c shows the modeling result of the field spectral $\Delta\Phi$ index. Strong relationships ($R^2 = 0.75$) also exist between the hyperspectral index and Chla concentration.

As shown in Fig. 4b, the satellite NCI' model could explain 76% of the total Chla variance, and the RMSE decreased to 6.38 μg/L. The R^2 of the NCI' model based on field spectral data (Fig. 4d) exceeded 0.8, which was higher than that of the satellite NCI' model, showing the validity of the established NCI' model and that this model has sufficient accuracy for practical Chla concentration estimation.

A comparison of the results of the four models reveals that all models showed good correlation between the Chla concentration and the spectral index derived from GF-1 data, and the precision of the IFB model, with a determination coefficient up to 0.96, was higher than that of the other models, while the R^2 of the ETB and $\Delta\Phi$ models were both above 0.80.
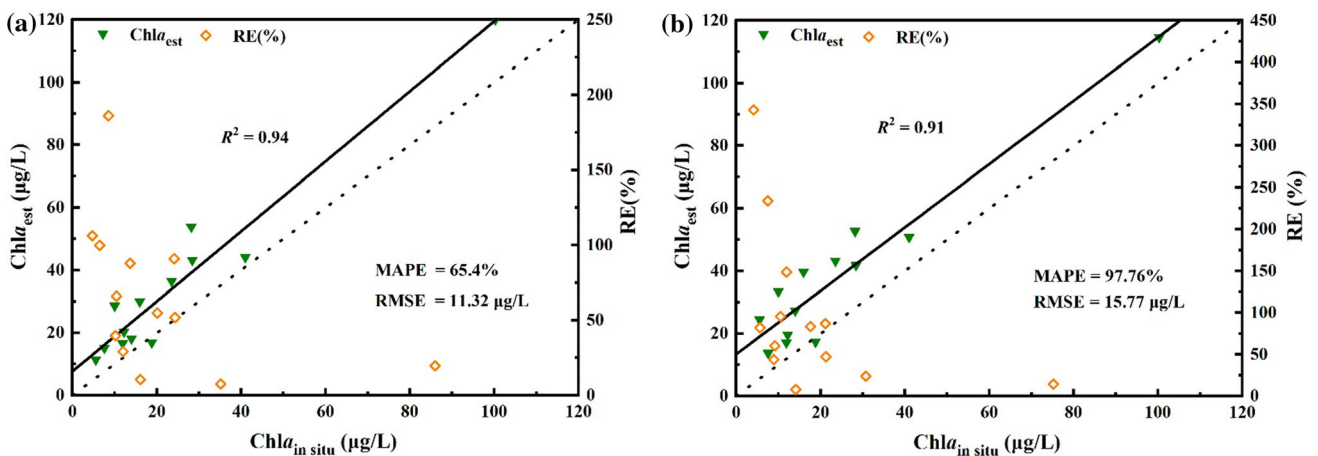
Model Validation

For evaluating the accuracy and stability of the established models, the assessment indexes of the GF-1 validation model used included the RE, MAPE and RMSE. A comparison between the satellite-estimated values and the values measured in situ is shown in Fig. 5. The estimated values of the ETB model were all adjacent to the diagonal lines, and the RMSE was less than 7.42 μg/L (Fig. 5a), which suggests that the model can perform well for Chla estimation in our study area. Figure 5b shows the validation results for the IFB model using GF-1 satellite data. The coefficient of determination reached 0.85, and the RMSE was only 5.20 μg/L, reflecting the highest model accuracy and stability.

For the semi-empirical model, the estimated results based on the field spectral data were better than those based on the satellite data. The validation accuracy of the $\Delta\Phi$ model was $R^2 = 0.94$ (Fig. 6a). Figure 6b shows the validation result of the NCI' model based on field spectral data, and the accuracy of the model exceeded 0.91. In contrast, Fig. 6c shows the validation result of the $\Delta\Phi$ model based on GF-1 satellite data. The R^2 of the model exceeded 0.67, and the estimated values of Chla were higher than the values measured in situ. Figure 6d shows the result of the validation of the NCI' model using GF-1 satellite data. The coefficient (R^2) of the model exceeded 0.66. The four models produce most of their error at low Chla values because suspended matter or other organic matter has a significant impact on the satellite reflectance of the lake water (Zhou et al., 2014). The IFB index based on the model calibration and validation with field spectra and GF-1 satellite data showed sufficient model accuracy and stability for the operational monitoring of the inland lake water. Therefore, the IFB model could be used to estimate
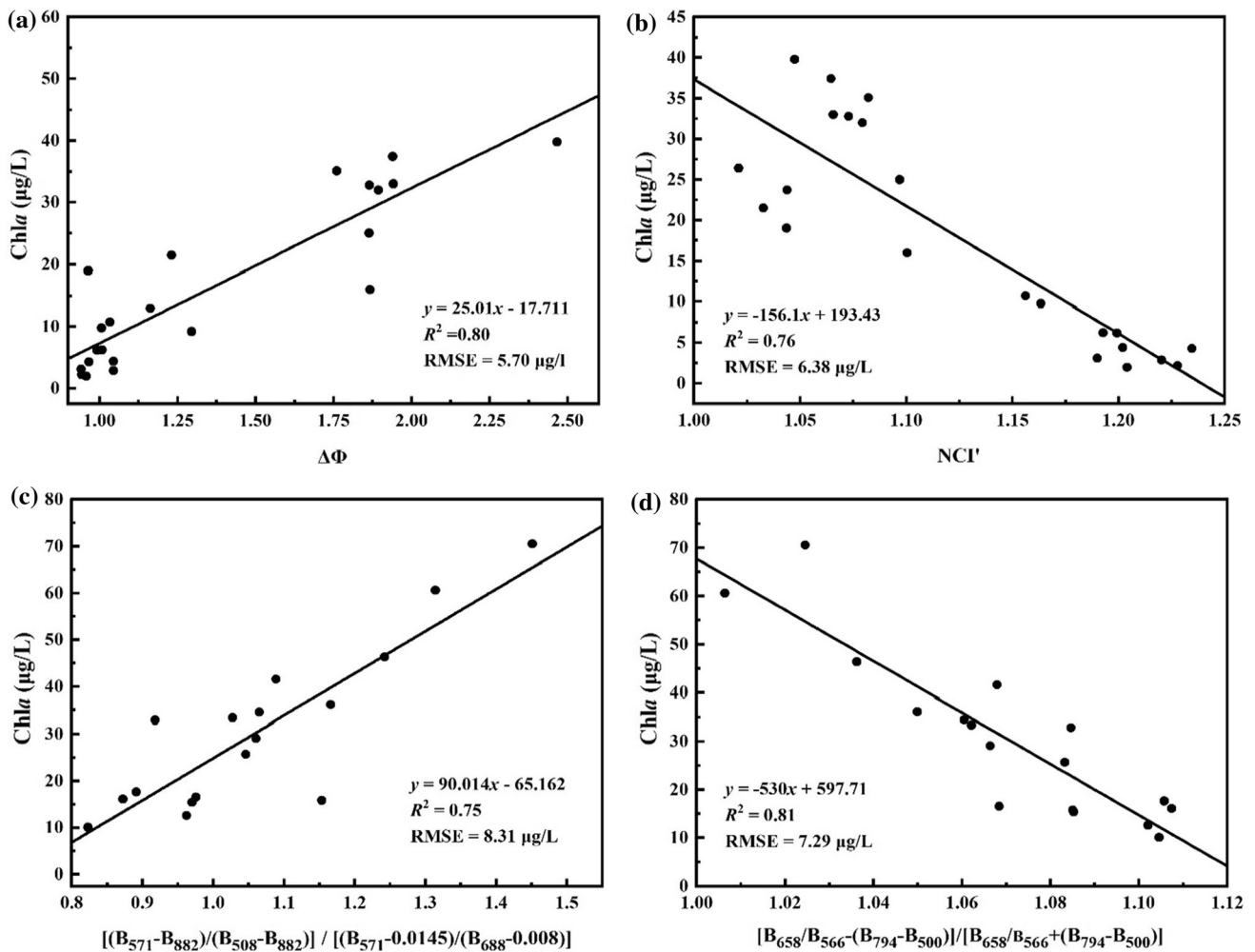
Fig. 4 The calibration of semi-analytical models based on GF-1 data and field spectra data: **a** calibration of the $\Delta\Phi$ model; **b** calibration of the NCI' model; **c** calibration of the field spectral $\Delta\Phi$ model; **d** calibration of the field spectral NCI' model

Fig. 5 The validation of the four-band combined model based on GF-1 satellite data: **a** Validation of the ETB model; **b** validation of the IFB model

and analyze the spatial distribution of Chla in our study area.

Spatial Analysis of the Chla Concentrations in Lake Dianshan

The IFB model was used to calculate the spatial distribution of the Chla concentration in Lake Dianshan for the typical days in years 2013–2017. As shown in the spatial distribution maps (Fig. 7), the Chla values were generally low in the middle of the lake and high in the northeast area and the coastal zone. This phenomenon mainly occurred because the inlets of the lake are located in the southwest, which leads to long-term deposition of nutrients in the northeast area of the lake (Liu et al., 2014; Wang et al., 2015). On the other hand, the main types of pollution in Lake Dianshan are domestic stockbreeding pollution and agricultural nonpoint source pollution. A large amount of cultivated land and many residential buildings are located in the northeast area of the lake, which has led to higher concentrations of nitrogen, phosphorus and Chla in that
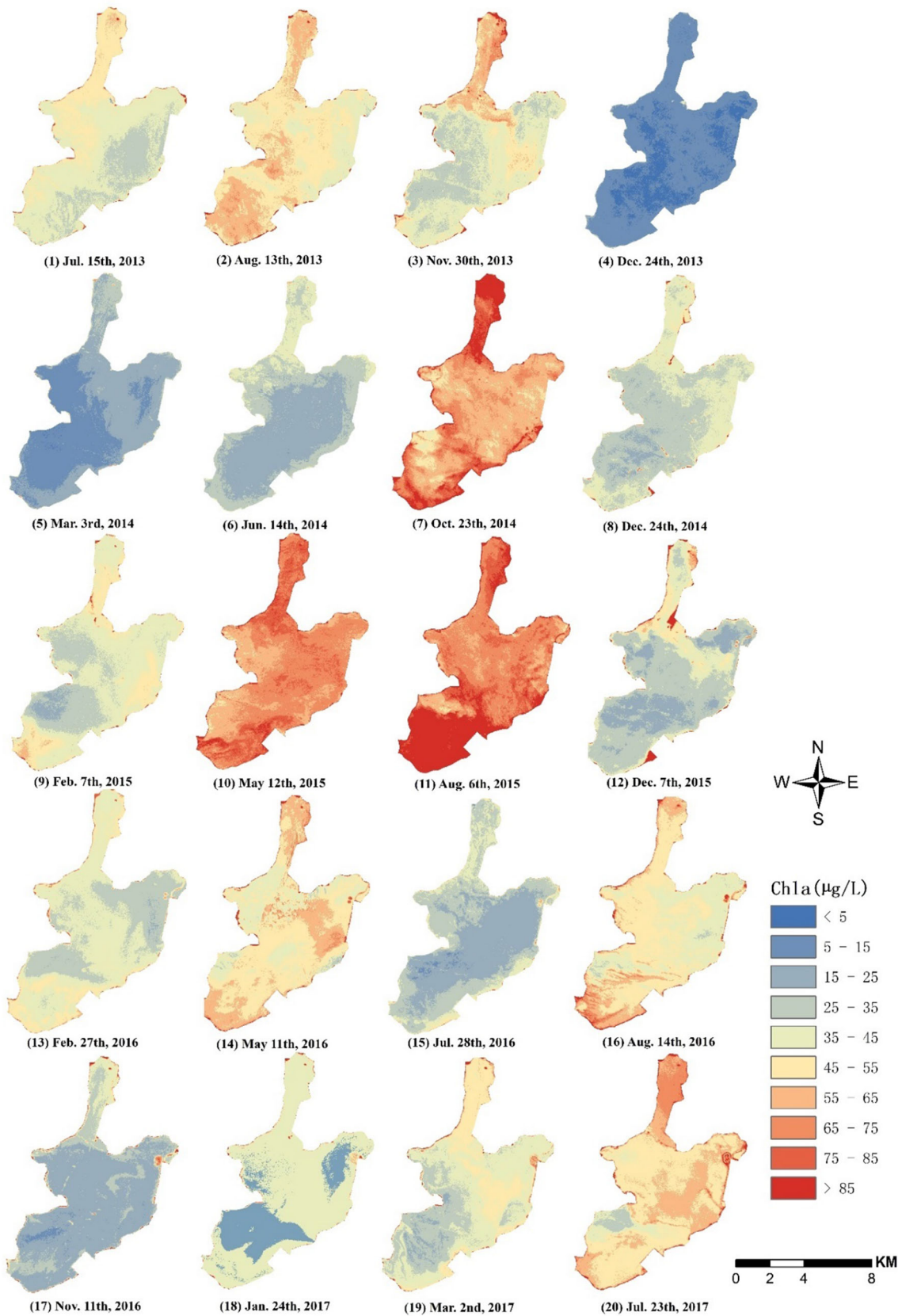
area (Wang et al., 2015). In total, the results estimated from the GF-1 satellite data were consistent with the synchronous Chla concentrations measured in situ (Xiong et al., 2017). Therefore, using the well-established IFB model of this paper, the spatial distribution of Chla concentrations can be explicitly described by the GF-1 high-spatial-resolution satellite data.

The proportions of the lake with different levels of Chla were analyzed based on the estimated Chla concentrations in 2013–2017. As shown in Fig. 8, we could distinguish and deduce the trophic state of the lake water. The lowest concentration of Chla occurred on December 4th, 2013, when the Chla concentration in the southwest lake area was below 2 μg/L and the proportion of the lake with a Chla concentration less than 10 μg/L was 79.49%. The proportion of the lake with a Chla concentration from 10 to 20 μg/
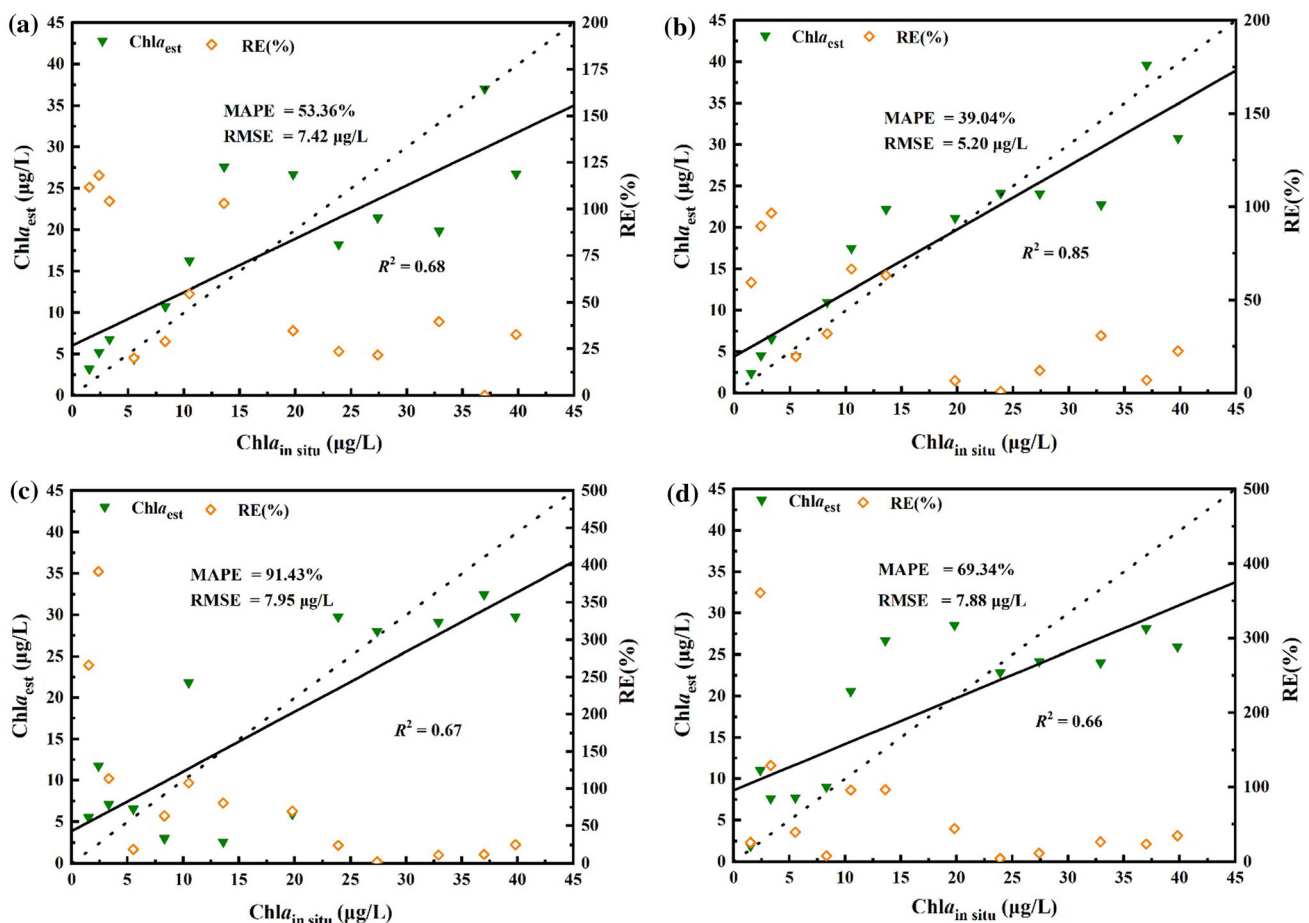

Fig. 6 The validation of the four-band combined model based on GF-1 satellite data: **a** validation of the field spectral $\Delta\Phi$ model; **b** validation of the field spectral NCI' model; **c** validation of the $\Delta\Phi$ model; **d** validation of the NCI' model

(1) Jul. 15th, 2013   (2) Aug. 13th, 2013   (3) Nov. 30th, 2013   (4) Dec. 24th, 2013

(5) Mar. 3rd, 2014   (6) Jun. 14th, 2014   (7) Oct. 23th, 2014   (8) Dec. 24th, 2014

(9) Feb. 7th, 2015   (10) May 12th, 2015   (11) Aug. 6th, 2015   (12) Dec. 7th, 2015

(13) Feb. 27th, 2016   (14) May 11th, 2016   (15) Jul. 28th, 2016   (16) Aug. 14th, 2016

(17) Nov. 11th, 2016   (18) Jan. 24th, 2017   (19) Mar. 2nd, 2017   (20) Jul. 23th, 2017

Chla (µg/L)

< 5
5 – 15
15 – 25
25 – 35
35 – 45
45 – 55
55 – 65
65 – 75
75 – 85
> 85

Fig. 8 Proportion of the lake area with different concentrations of Chla and average Chla concentrations based on GF-1 satellite data from 2013 to 2017
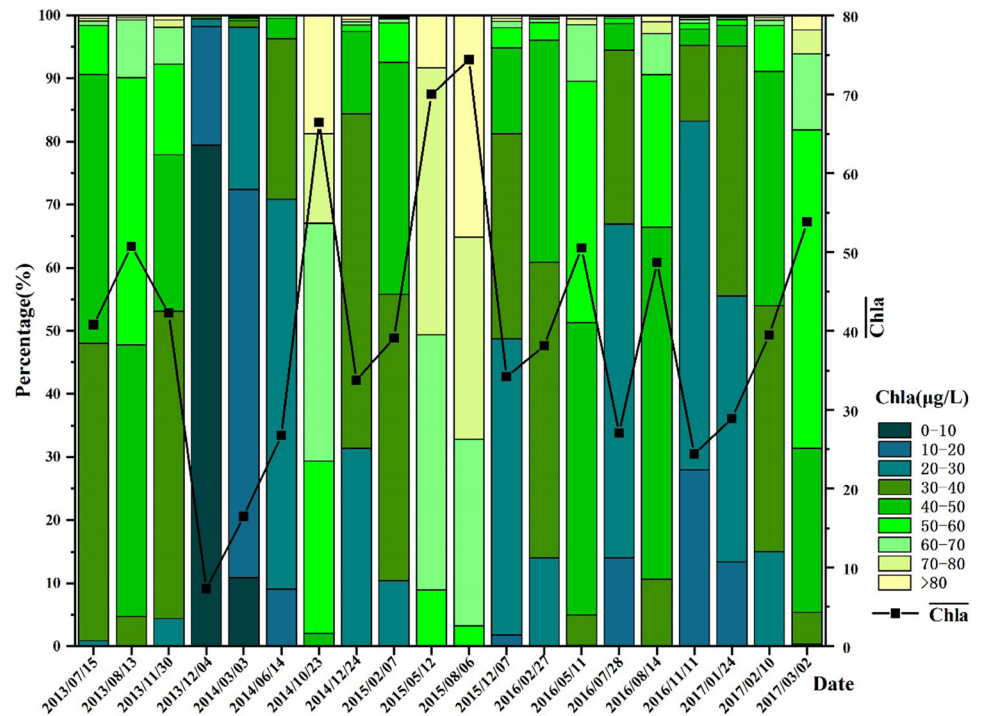
L was only 18.74% and was concentrated in the northeast part of the lake, which implies that Lake Dianshan was in a state between oligotrophic and mesotrophic. On June 14th, 2014, the concentration of Chla in most lake areas was higher than 20 µg/L, and the proportion of the lake area with this concentration exceeded 81%, which indicated that the lake water was at a status between mesotrophic and eutrophic. The highest concentration of Chla appeared on August 6th, 2015, when almost all Chla concentrations in the lake were higher than 35 µg/L. Moreover, lake areas with a concentration of Chla higher than 70 µg/L accounted for 67.21% of the total area, which indicates serious eutrophication and the potential for an algal bloom. According to the estimated results calculated by using GF-1 satellite data for the years 2013–2017, it can be concluded that water quality needs to be controlled, and continuous monitoring is thus essential for this lake (Xiong et al., 2017). Furthermore, we can see that high Chla events always occurred in May–October, which indicated that the variation in the Chla concentration had obvious seasonality. This was because the values of TN, TP, and other nutrients reached to the threshold and the water temperatures exceeded 20 °C during the summer months, which promoted and accelerated the increasing of the Chla (Xu et al., 2015).

Discussion

Analysis and comparison of the estimated results of the model based on the GF-1 satellite data revealed that the accuracy of the four models all exceeded 76%, which indicates that these models can effectively infer the concentration of Chla in the study area (Table 2). As far as the validation results of the model are concerned, the values estimated by each model are basically evenly distributed on both sides of the diagonal lines in the comparison, and all of them have good stability. However, there were still differences in the estimation by the different models. The modeling accuracy of the NCI' model and $\Delta\Phi$ model was slightly unstable, with $R^2 = 0.67$ and 0.66, respectively. In summary, according to the GF-1 satellite data, the IFB model has the best model accuracy and stability, which is equivalent to the estimation accuracy ($R^2 = 0.737$) of the GSM algorithm recommended by IOCCG (Lee, 2006). It indicates that the new IFB model could be applied to GF-1 satellite data with satisfactory model accuracy.

The GF-1 satellite imagery integrated with semi-empirical methods such as the $\Delta\Phi$ algorithm used to retrieve Chla concentrations should be further developed (Chao Rodriguez et al., 2014; Pyo et al., 2016), probably because of the complexity involved in modeling the radiation transfer equation in water (Arabi et al., 2016; Tilstone et al., 2011). However, empirical models require statistical analysis techniques only, which are easier to handle and

Table 2 The accuracy results of the four established models

Model	R^2		MAPE (%)		RMSE (μg/L)	
	Calibration	Validation	Calibration	Validation	Calibration	Validation
ETB model	0.87	0.68	35.82	53.36	4.65	7.42
$\Delta\Phi$ model	0.80	0.67	56.60	91.43	5.70	7.95
IFB model	0.96	0.85	29.26	39.04	2.69	5.20
NCI' model	0.76	0.66	39.99	69.34	6.38	7.88

may give results as good as those of the semi-analytical models, even though the empirical results sometimes lack consistency and frequently need in situ data to correct the model (Ma & Dai, 2005).

In terms of the accuracy of each model, differences between the models built using the GF-1 data and the field hyperspectral measurements existed for two reasons. One is that the GF-1 WFV sensor can detect the spectral reflectance in only the four bands and cannot cover the specific spectral regions sensitive to the variance in the Chla concentration (Li et al., 2015). The other is that the results of the atmospheric correction (Fig. S1) and the geometric correction determine the accuracy of the spectral reflectance derived from the GF-1 satellite imagery (Wu et al., 2015). Further studies will explore the specific impacts of atmospheric corrections on the IFB index. The GF-1-derived Chla concentration closely followed the field records. However, challenges remain in validating the algorithm for universal application to different study areas. Note that the water in different lakes may have different inherent optical properties, and more field measurements and remote sensing data from different study areas are necessary to investigate potential improvements to the model.

The result has shown that GF-1 satellite data can be used quantitatively to estimate the concentrations of Chla, and further applications of the GF-1 data will allow the hindcasting of biophysical parameters in small ponds and lakes. The GF-1 historical archives are helpful in tracing the eutrophic status of lake water and may produce some useful time series of environmental information (Liu et al., 2014). From the time series of the spatial distribution of Chla in Lake Dianshan, we could discover the detailed local changes in the Chla concentration and the Chla evolution in the lake; this will be useful for the prediction of a lake's trophic status and the possibility of algal blooms.

Conclusions

In this research, high-resolution GF-1 satellite data and field spectra were used to construct an operational model to estimate the Chla concentration in Lake Dianshan and to deeply investigate the applicability of high-spatial-resolution satellite data in the field to water quality retrieval for small and medium-sized inland lakes. For the IFB model based on GF-1 satellite data, the RE of the estimated Chla concentration was 29.26% on average, and the RMSE was only 2.69 μg/L. The high accuracy indicates that the IFB model can be applied to the estimation of the Chla concentration in small inland lakes. Validation models based on a different dataset also verified the accuracy and practicability of the established models. It was shown that the GF-1 satellite data could be effectively used to estimate the concentration of Chla. Because of the high spatial and temporal resolution of the GF-1 satellite, which serves as the key factor for inland water quality assessment, GF-1 satellite data may have a great potential in small to medium-sized inland water body monitoring.

Declarations

Conflict of interest The authors declare that they have no conflict of interest. This article does not contain any studies with human participants or animals performed by any of the authors. Informed consent was obtained from all individual participants included in the study.

References

Allan, M. G., Hamilton, D. P., Hicks, B., & Brabyn, L. (2015). Empirical and semi-analytical chlorophyll a algorithms for multi-temporal monitoring of New Zealand lakes using Landsat. *Environmental Monitoring & Assessment, 187*, 1–24.

Arabi, B., Salama, M., Wernand, M., & Verhoef, W. (2016). MOD2SEA: A coupled atmosphere-hydro-optical model for the retrieval of chlorophyll-a from remote sensing observations in complex turbid waters. *Remote Sensing, 8*, 722.

Carter, G. A., & Knapp, A. K. (2001). Leaf optical properties in higher plants: Linking spectral characteristics to stress and chlorophyll concentration. *American Journal of Botany, 88,* 677–684.

Chao Rodriguez, Y., Anjoumi, A., Gómez, J., Pérez, D., & Rico, E. (2014). Using Landsat image time series to study a small water body in Northern Spain. *Environmental Monitoring and Assessment, 186,* 3511–3522.

Chen, J., Quan, W., Wen, Z., & Cui, T. (2013). An improved three-band semi-analytical algorithm for estimating chlorophyll- a concentration in highly turbid coastal waters: A case study of the Yellow River estuary, China. *Environmental Earth Sciences, 69,* 2709–2719.

Cheng, C., Wei, Y., Lv, G., & Yuan, Z. (2013). Remote estimation of chlorophyll-a concentration in turbid water using a spectral index: A case study in Taihu Lake, China. *Journal of Applied Remote Sensing, 7,* 073465.

Choe, E., Lee, J. W., & Cheon, S. U. (2015). Monitoring and modelling of chlorophyll-a concentrations in rivers using a high-resolution satellite image: A case study in the Nakdong river, Korea. *International Journal of Remote Sensing, 36,* 1645–1660.

Dall'Olmo, G., & Gitelson, A. A. (2005). Effect of bio-optical parameter variability on the remote estimation of chlorophyll-a concentration in turbid productive waters: experimental results. *Applied Optics, 44,* 412–422.

Duan, H., Ma, R., Zhang, Y., Loiselle, S. A., Xu, J., Zhao, C., Zhou, L., & Shang, L. (2010). A new three-band algorithm for estimating chlorophyll concentrations in turbid inland lakes. *Environmental Research Letters, 5,* 044009.

Ekercin, S. (2007). Water quality retrievals from high resolution Ikonos multispectral imagery: A case study in Istanbul, Turkey. *Water Air & Soil Pollution, 183,* 239–251.

Feng, Q., Gong, J., Wang, Y., Liu, J., Li, Y., Ibrahim, A. N., Liu, Q., & Hu, Z. (2015). Estimating chlorophyll-a concentration based on a four-band model using field spectral measurements and HJ-1A hyperspectral data of Qiandao Lake, China. *Remote Sensing Letters, 6,* 735–744.

Fichot, C. G., Downing, B. D., Bergamaschi, B. A., Windham-Myers, L., Marvin-DiPasquale, M., Thompson, D. R., & Gierach, M. M. (2016). High-resolution remote sensing of water quality in the San Francisco Bay-delta estuary. *Environmental Science & Technology, 50,* 573–583.

Giardino, C., Bresciani, M., Cazzaniga, I., Schenk, K., Rieger, P., Braga, F., Matta, E., & Brando, V. E. (2014). Evaluation of multi-resolution satellite sensors for assessing water quality and bottom depth of Lake Garda. *Sensors, 14,* 24116–24131.

Gitelson, A. A., Dall'Olmo, G., Moses, W., Rundquist, D. C., Barrow, T., Fisher, T. R., Gurlin, D., & Holz, J. (2008). A simple semi-analytical model for remote estimation of chlorophyll-a in turbid waters: Validation. *Remote Sensing of Environment, 112,* 3582–3593.

Gons, H. J. (2005). Remote sensing of the cyanobacterial pigment phycocyanin in turbid inland water. *Limnology & Oceanography, 50,* 237–245.

González Vilas, L., Spyrakos, E., & Torres Palenzuela, J. M. (2011). Neural network estimation of chlorophyll a from MERIS full resolution data for the coastal waters of Galician rias (NW Spain). *Remote Sensing of Environment, 115,* 524–535.

Han, Q. J., Fu, Q. Y., Zhang, X. W., & Liu, L. (2014). High-frequency radiometric calibration for wide field-of-view sensor of GF-1 satellite. *Optics & Precision Engineering, 22,* 1707–1714.

Hu, C., Chen, Z., Clayton, T. D., Swarzenski, P., Brock, J. C., & Muller-Karger, F. E. (2004). Assessment of estuarine water-quality indicators using MODIS medium-resolution bands: Initial results from Tampa Bay, FL. *Remote Sensing of Environment, 93,* 423–441.

Kloiber, S. M., Brezonik, P. L., & Bauer, M. E. (2002). Application of landsat imagery to regional-scale assessments of lake clarity. *Water Research, 36,* 4330–4340.

Le, C., Li, Y., Zha, Y., Sun, D., Huang, C., & Lu, H. (2009). A four-band semi-analytical model for estimating chlorophyll a in highly turbid lakes: The case of Taihu Lake, China. *Remote Sensing of Environment, 113,* 1175–1182.

Lee, Z. (2006). Remote sensing of inherent optical properties: Fundamentals, tests of algorithms and applications. Reports of the International Ocean-Colour Coordination Group, no. 5, IOCCG, Dartmouth, Canada.

Li, J., Chen, X., Tian, L., Huang, J., & Feng, L. (2015). Improved capabilities of the Chinese high-resolution remote sensing satellite GF-1 for monitoring suspended particulate matter (SPM) in inland waters: Radiometric and spatial considerations. *ISPRS Journal of Photogrammetry and Remote Sensing, 106,* 145–156.

Lin, C., Li, Y., Yuan, Z., Lau, A. K. H., Li, C., & Fung, J. C. H. (2015). Using satellite remote sensing data to estimate the high-resolution distribution of ground-level PM2.5. *Remote Sensing of Environment, 156,* 117–128.

Liu, X., Wu, Z., Xu, H., Zhu, H., Wang, X., & Liu, Z. (2014). Assessment of pollution status of Dalianhu water sources in Shanghai, China and its pollution biological characteristics. *Environmental Earth Sciences, 71,* 4543–4552.

Ma, R., & Dai, J. (2005). Investigation of chlorophyll-a and total suspended matter concentrations using Landsat ETM and field spectral measurement in Taihu Lake, China. *International Journal of Remote Sensing, 26,* 17.

Myint, S. W., Gober, P., Brazel, A., Grossman-Clarke, S., & Weng, Q. (2011). Per-pixel vs. object-based classification of urban land cover extraction using high spatial resolution imagery. *Remote Sensing of Environment, 115,* 1145–1161.

Pyo, J. C., Ha, S. H., Pachepsky, Y. A., Lee, H., Ha, R., Nam, G., Kim, M. S., Im, J., & Cho, K. H. (2016). Chlorophyll-concentration estimation using three difference bio-optical algorithms, including a correction for the low-concentration range: The case of the Yiam reservoir, Korea. *Remote Sensing Letters, 7,* 407–416.

Sarris, A., Papadopoulos, N., Agapiou, A., Salvi, M. C., Hadjimitsis, D. G., Parkinson, W. A., Yerkes, R. W., Gyucha, A., & Duffy, P. R. (2013). Integration of geophysical surveys, ground hyper-spectral measurements, aerial and satellite imagery for archae-ological prospection of prehistoric sites: The case study of Vésztő-Mágor Tell, Hungary. *Journal of Archaeological Science, 40,* 1454–1470.

Schalles, J. F., G.A.A., Yacobi Y Z, et al. (1998). Estimation of chlorophyll a from time series measurements of high spectral resolution reflectance in an eutrophic lake. *Journal of Phycology, 34,* 383–390.

Sun, D., Li, Y., Le, C., Shi, K., Huang, C., Gong, S., & Yin, B. (2013). A semi-analytical approach for detecting suspended particulate composition in complex turbid inland waters (China). *Remote Sensing of Environment, 134,* 92–99.

Tian, L., Wai, O. W. H., Chen, X., Li, W., Li, J., Li, W., & Zhang, H. (2016). Retrieval of total suspended matter concentration from Gaofen-1 wide field imager (WFI) multispectral imagery with the assistance of Terra MODIS in turbid water—case in Deep Bay. *International Journal of Remote Sensing, 37,* 3400–3413.

Tilstone, G. H., Angel-Benavides, I. M., Pradhan, Y., Shutler, J. D., Groom, S., & Sathyendranath, S. (2011). An assessment of chlorophyll-a algorithms available for SeaWiFS in coastal and open areas of the Bay of Bengal and Arabian Sea. *Remote Sensing of Environment, 115,* 2277–2291.

Wang, J., Yuan, Q., & Xie, B. (2015). Temporal dynamics of cyanobacterial community structure in Dianshan Lake of Shanghai, China. *Annals of Microbiology, 65*, 105–113.

Watanabe, F., Alcântara, E., Rodrigues, T., Imai, N., Barbosa, C., & Rotta, L. (2015). Estimation of chlorophyll-a concentration and the trophic state of the Barra Bonita hydroelectric reservoir using OLI/Landsat-8 images. *International Journal of Environmental Research and Public Health, 12*, 10391.

Watanabe, F., Mishra, D. R., Astuti, I., Rodrigues, T., Alcântara, E., Imai, N. N., & Barbosa, C. (2016). Parametrization and calibration of a quasi-analytical algorithm for tropical eutrophic waters. *Isprs Journal of Photogrammetry & Remote Sensing, 121*, 28–47.

Wu, X., & Cheng, Q. (2010). *Estimation of chlorophyll a and total suspended matter concentration using Quickbird image and in situ spectral reflectance in Hangzhou Bay*. SPIE.

Wu, M., Huang, W., Niu, Z., & Wang, C. (2015). Combining HJ CCD, GF-1 WFV and MODIS data to generate daily high spatial resolution synthetic data for environmental process monitoring. *International Journal of Environmental Research and Public Health, 12*, 9920.

Xiong, G., Wang, G., Wang, D., Yang, W., Chen, Y., & Chen, Z. (2017). Spatio-temporal distribution of total nitrogen and phosphorus in Dianshan Lake, China: the external loading and self-purification capability. *Sustainability, 9*, 500.

Xu, H., Paerl, H. W., Qin, B., Zhu, G., Hall, N. S., & Wu, Y. (2015). Determining critical nutrient thresholds needed to control harmful cyanobacterial blooms in eutrophic Lake Taihu, China. *Environmental Science and Technology, 49*, 1051–1059.

Yang, A., Bo, Z., Wenbo, L., Shanlong, W., & Qinhuo, L. (2015). Cross-calibration of GF-1/WFV over a desert site using Landsat-8/OLI imagery and ZY-3/TLC data. *Remote Sensing, 7*, 10763–10787.

Zhou, L., Ma, W., Zhang, H., Li, L., & Tang, L. (2015). Developing a PCA–ANN model for predicting chlorophyll a concentration from field hyperspectral measurements in Dianshan Lake, China. *Water Quality Exposure & Health, 7*, 1–12.

Zhou, L., Roberts, D. A., Ma, W., Zhang, H., & Tang, L. (2014). Estimation of higher chlorophylla concentrations using field spectral measurement and HJ-1A hyperspectral satellite data in Dianshan Lake, China. *ISPRS Journal of Photogrammetry and Remote Sensing, 88*, 41–47.

Zhou, L., Xu, B., Ma, W., Zhao, B., Li, L., & Huai, H. (2013). Evaluation of hyperspectral multi-band indices to estimate chlorophyll-A concentration using field spectral measurements and satellite data in Dianshan Lake, China. *Water, 5*, 525–539.

Zou, W., Yuan, L., & Zhang, L. (2013). Analyzing the spectral response of submerged aquatic vegetation in a eutrophic lake, Shanghai, China. *Ecological Engineering, 57*, 65–71.